Available online at www.sciencedirect.com
ScienceDirect
International Journal of Heat and Mass Transfer 50 (2007) 2051–2059
International Journal of HEAT and MASS TRANSFER
www.elsevier.com/locate/ijhmt

Heat transfer and entropy generation optimization of forced convection in porous-saturated ducts of rectangular cross-section

K. Hooman [a,*], H. Gurgenci [a], A.A. Merrikh [b]

[a] School of Engineering, The University of Queensland, Brisbane, Qld 4072, Australia
[b] Advanced Micro Devices, 5204 E. Ben White Boulevard, Austin, TX, 78741, United States

Received 22 July 2006; received in revised form 11 November 2006
Available online 16 January 2007

Abstract

We investigate analytically the first and the second law characteristics of fully developed forced convection inside a porous-saturated duct of rectangular cross-section. The Darcy–Brinkman flow model is employed. Three different types of thermal boundary conditions are examined. Expressions for the Nusselt number, the Bejan number, and the dimensionless entropy generation rate are presented in terms of the system parameters. The conclusions of this analytical study will make it possible to compare, evaluate, and optimize alternative rectangular duct design options in terms of heat transfer, pressure drop, and entropy generation.

Keywords: Entropy generation; Porous media; Forced convection; Rectangular duct

1. Introduction

There has recently been renewed interest in the problem of forced convection in porous media. An increasingly important application is in liquid cooled electronics with coolants such as water or poly-α-olefin flowing through aluminum porous metal matrix assemblies. Narasimhan and Lage [1] offer an analysis of forced convection through an aluminum based porous matrix heated from top and bottom to model the heat generated by the electronic circuits in radar equipment. Commensurate with the generic importance of the area, a substantial amount of literature on this topic is already available as reported in Nield and Bejan [2] and Cheng [3]. Circular tubes or semi-infinite parallel plate channels are the most widely used geometries in electronics cooling equipment having either clear fluid or porous matrices such as water distribution systems, heat exchangers, liquid cooled cold plates, and similar applications. Fluid flow and heat transfer characteristics of such problems have been analyzed in detail for various boundary conditions.

Considering circular tubes or parallel plate geometries, the simplicity of the geometry allows analytical solution of closed form. Thus the question naturally arises as to whether analytical solutions for more complicated cross-sections are possible. The method of weighted residuals was exploited by Haji-Sheikh and Vafai [4] in their study of thermally developing convection in ducts of various shapes. In a subsequent study, Haji-Sheikh [5] has applied Fourier series method to investigate fully developed forced convection in a duct of rectangular cross-section. Haji-Sheikh et al. [6–10] have investigated heat transfer through porous ducts of arbitrary cross-sections. Their focus was to find heat transfer characteristics of the thermal entrance region. Applying Fourier series method, Hooman and Merrikh [11] have analytically investigated heat transfer and fluid flow in a rectangular duct occupied by a hyper-porous medium. In ducts of arbitrary cross-section, Hooman [12,13] and Hooman and Gurgenci [14] have reported closed form solutions for the fully developed

* Corresponding author. Tel.: +61 7 33653668; fax: +61 7 33654799.
E-mail address: k.hooman@uq.edu.au (K. Hooman).

0017-9310/$ - see front matter © 2006 Elsevier Ltd. All rights reserved.
doi:10.1016/j.ijheatmasstransfer.2006.11.015

Nomenclature

a	channel width to height ratio
A	parameter defined by Eq. (2b)
A_1, A_2	constants
B^*	parameter defined by Eq. (27)
Be	Bejan number, Eq. (6d)
Br	Darcy–Brinkman number $\frac{\mu U^2 H}{q'' K}$
Br^*	modified Brinkman number $\frac{\mu U^2}{kT_w q^{*2}}$
c_P	specific heat at constant pressure (J/kg K)
Da	Darcy number K/H^2
D_H	hydraulic diameter $4Ha/(a+1)$ (m)
D_n	coefficient defined by Eq. (2c)
FFI	fluid friction irreversibility per unit volume (W/m^3 K)
F_n	coefficients defined by Eq. (25)
G	negative of the applied pressure gradient (Pa/m)
H	half channel width (m)
HTI	heat transfer irreversibility per unit volume (W/m^3 K)
k	porous medium thermal conductivity (W/m^2 K)
K	permeability (m^2)
K_n	coefficients defined by Eq. (19)
m	parameter $(s^2+\lambda_n^2)^{1/2}$
M	viscosity ratio
Ns	dimensionless entropy generation Eq. (9)
Ns^*	cross-sectional average of Ns
Nu	Nusselt number defined by Eqs. (5a) and (5b)
Nu_i	Nusselt number for the boundary condition case i ($i=1,2,3$)
P	duct perimeter $P=4H(1+a)$ (m)
P_h	heated perimeter of the duct (m)
Pe	the Péclet number $Pe=\rho c_p U D_H/k$
q'	wall heat transfer rate per unit length of the duct (W/m)
q''	heat transfer rate per unit heat transfer area of the duct Eq. (5b) (W/m^2)
q^*	dimensionless heat flux, Eq. (10)
S	porous media shape parameter $s=(MDa)^{-1/2}$
$\dot{S}_{gen}$	entropy generation rate per unit volume (W/m^3 K)
T^*	local absolute temperature (K)
T_m	bulk temperature (K)
T_w	wall temperature (K)
u^*	x-velocity (m/s)
$\hat{u}$	dimensionless velocity equation (2a)
U	average velocity (m/s)
x^*	longitudinal coordinate (m)
x	dimensionless coordinate, $(x^*/H)/Pe$
y^*, z^*	coordinates (m)
y, z	$(y^*,z^*)/H$

Greek symbols

θ	dimensionless temperature
θ_b	dimensionless bulk temperature
λ_n	eigenvalues
μ	fluid viscosity (N s/m^2)
$\tilde{\mu}$	effective viscosity (N s/m^2)
ρ	fluid density (kg/m^3)
ϕ	dimensionless viscous dissipation function

temperature distribution and the Nusselt number as well as local entropy generation rate by applying the Darcy momentum equation.

The groundbreaking work by Bejan [15] introduced the concept of entropy generation analysis due to fluid flow and heat transfer as a powerful tool to optimize variety of configurations when analyzing engineering problems. Since entropy generation destroys the work availability of a system, it makes good engineering sense to focus on irreversibility of heat transfer and fluid flow processes to understand the associated entropy generation mechanisms. The literature on the topic is rich for clear fluids through unobstructed ducts. A recent survey of literature on the topic can be found in [16,17].

Modeling entropy generation in porous media is comparatively more tedious than clear fluid case due to the increased number of variables present in governing equations. For the Darcy flow model, viscous dissipation can be modeled via velocity square term only (see for example Baytas [18,19] or Hooman [12,13]). But when the boundary and inertia effects are to be included, there are three alternatives for viscous dissipation term. Nield [20] argued that the viscous dissipation function should remain equal to the power of the drag force when the Brinkman equation is considered. On the other hand, Al-Hadrami et al. [21] have proposed a clear flow compatible model. Nield et al. [22] have combined the three alternatives to a single equation treating both the isothermal and isoflux boundary conditions. A similar attempt was made by Hooman et al. [23,24] for a developing flow. Nield [25] has commented on the alternative models applied so far, emphasizing that one should not use just the term involving velocity derivatives. In the light of Nield [25], Hooman and Ejlali [26] and Hooman et al. [27] have questioned some of the articles that neglected the Darcy dissipation term. Hence, further work on modeling entropy generation in a porous medium is called for.

Energy–entropy analysis for ducts of arbitrary cross-section is already studied in [12–14] by applying the Darcy flow model. However, when non-Darcy effects are considered, the velocity distribution has no longer a uniform (slug) shape and the situation gets more complicated. Applying the velocity distribution reported in [11], this paper offers an analytical solution of heat transfer and

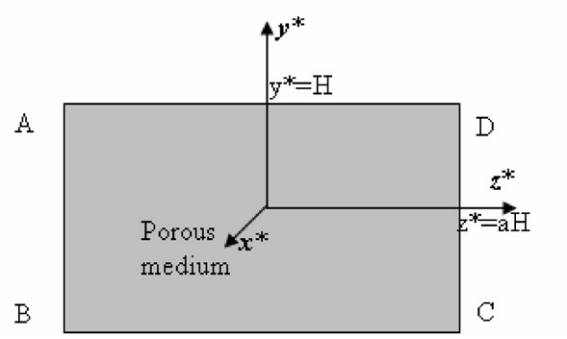

Fig. 1. Definition sketch.

Table 1
Case definition in terms of boundary conditions

Case	Entity name	Boundary condition	P_h/P
1	AB, BC, CD, DA	Heated	1
2	CD	Insulated	$\frac{1+2a}{2+2a}$
	AB,BC, DA	Heated	
3	BC, AD	Heated	$\frac{a}{1+a}$
	AB, CD	Insulated	

entropy generation in a duct of rectangular cross-section saturated by a porous medium. In the terminology of Shah and London [28], three cases of **H1** boundary condition are applied, to be referred to as cases 1, 2, and 3 as described in Fig. 1 and Table 1. For **H1** boundary condition one assumes a constant longitudinal heat flux where in each cross-section the wall temperature is constant independent of other two dimensions. This boundary condition may represent, for example, electric resistance heating of highly conductive walls. In case 1, the four walls are uniformly heated. For this case we have adopted the results of [11] for both velocity and temperature profiles to investigate the second law aspects of the problem. In case 2, one of the walls is assumed to be adiabatic. In case 3, the two sidewalls are assumed to be adiabatic. To the authors' knowledge, no analytical solution is available for cases 2 and 3 of this problem.

2. Analysis

2.1. Hydrodynamic aspects of the problem

The Darcy–Brinkman extended momentum equation for the case of unidirectional (fully developed) flow in the x^*-direction in a rectangular duct occupied by a porous medium with velocity $u^*(y^*,z^*)$ can be written based on [2]

$$\tilde{\mu}\left(\frac{\partial^2 u^*}{\partial y^{*2}}+\frac{\partial^2 u^*}{\partial z^{*2}}\right)-\frac{\mu}{K}u^*+G=0. \tag{1}$$

In the above equation, μ is the fluid viscosity, $\tilde{\mu}$ is the effective viscosity (based on adoption of the Brinkman model), K is the permeability, and G is the negative of the applied pressure gradient. The analytical solution to this equation subject to impermeable wall boundary conditions is [11]

$$\hat{u}=\frac{1}{A}\sum_{n=1}^{\infty}D_n\left(1-\frac{\cosh mz}{\cosh ma}\right)\cos\lambda_n y, \tag{2a}$$

$$A=\frac{2}{\pi}\sum_{n=1}^{\infty}\frac{1}{(2n-1)^2m^2}\left(1-\frac{\tanh ma}{ma}\right), \tag{2b}$$

$$D_n=\frac{(-1)^{n-1}}{(2n-1)m^2}, \tag{2c}$$

where $(x,y,z)=(x^*/Pe,y^*,z^*)/H$ are the dimensionless coordinates, $M=\tilde{\mu}/\mu$ is the viscosity ratio, $Da=K/H^2$ is the Darcy number, $\lambda_n=(2n-1)\pi/2$ are the eigenvalues, $s=(MDa)^{-1/2}$ is the porous media shape parameter, $Pe=\rho c_p UD_H/k$ is the Péclet number, and $m=(s^2+\lambda_n^2)^{1/2}$. Here $\hat{u}$ is the dimensionless velocity defined as

$$\hat{u}=\frac{u^*}{U}, \tag{3}$$

where U is the average velocity defined as $U=\langle u^*\rangle$ (the angle brackets denote an average taken over the duct cross-section).

2.2. Energy–entropy analysis

2.2.1. First law aspects of the problem

Steady-state condition, local thermal equilibrium, homogeneity, and no thermal dispersion are assumed (one may consult [2] to find the condition based on which one can neglect the aforementioned effects in the thermal energy equation). In this case the thermal energy equation becomes

$$u^*\frac{\partial T^*}{\partial x^*}=\frac{k}{\rho c_P}\left(\frac{\partial^2 T^*}{\partial y^{*2}}+\frac{\partial^2 T^*}{\partial z^{*2}}\right). \tag{4a}$$

Here T^* is the temperature, ρ is the density of the fluid, c_P is the specific heat at constant pressure of the fluid, and k is the effective thermal conductivity of the medium.

Thermally fully developed condition with isoflux walls requires $\frac{\partial T^*}{\partial x^*}=\frac{dT_m}{dx^*}$, as noted by Shah and London [28]. On the other hand, the first law of thermodynamics, when applied to a thin cross-sectional slice of the duct (size Pdx^*), leads to the requirement that

$$\rho c_p AU\frac{\partial T^*}{\partial x^*}\,dx^*=q''\,dx^*P_h. \tag{4b}$$

Eq. (4b) shows that heat transfer from the walls to the stream reflects the enthalpy rise experienced by the stream assuming that the fluid is an ideal gas or an incompressible liquid with negligible pressure changes. Hence, the above equation can be rearranged as

$$\frac{\partial T^*}{\partial x^*}=\frac{4q''}{\rho c_p UD_H}\frac{P_h}{P}. \tag{4c}$$

In particular, in terms of a and H, Eq. (4c) takes the following form

$$\frac{\partial T^*}{\partial x^*}=\frac{q''(1+a)}{\rho c_p UHa}\frac{P_h}{P}. \tag{4d}$$

This is a general conclusion and can be applied for any of the three boundary conditions considered here (see the last column of Table 1). The Nusselt number is defined as

$$Nu = \frac{q'' D_H}{k(T_w^* - T_m)}, \tag{5a}$$

where q'' is the heat transfer rate per unit area of the duct similar to what defined by Shah and London [28] based on the heat flux defined as follows

$$q'' = \frac{q'}{P_h}. \tag{5b}$$

Here, q' is the wall heat transfer rate per unit length of the duct and P_h is the heated perimeter of the duct. Moreover, the bulk temperature is defined as $T_m = \langle \hat{u} T^* \rangle$ and the hydraulic diameter, D_H, is given by $D_H = 4Ha/(a+1)$.

2.2.2. Second law aspects of the problem

Entropy generation through heat and fluid flow in a porous medium is associated with thermodynamic irreversibility. Different sources are responsible for generation of entropy, including heat transfer across a finite temperature gradient, mixing, and viscous dissipation. Following Bejan [15], the entropy generation rate per unit volume (known as "entropy generation *hereafter*") is related to *heat transfer irreversibility* due to transfer in the direction of finite temperature gradients, HTI, and *fluid friction irreversibility* due to frictional heating, FFI, as

$$\dot{S}_{gen} = \mathrm{HTI} + \mathrm{FFI}. \tag{6a}$$

According to [6,7,15,21] the above terms are defined as

$$\mathrm{HTI} = k \frac{\left(\frac{\partial T^*}{\partial x^*}\right)^2 + \left(\frac{\partial T^*}{\partial y^*}\right)^2 + \left(\frac{\partial T^*}{\partial z^*}\right)^2}{T^{*2}}, \tag{6b}$$

$$\mathrm{FFI} = \frac{\frac{\mu u^{*2}}{K} + \tilde{\mu}\left(\left(\frac{\partial u^*}{\partial y^*}\right)^2 + \left(\frac{\partial u^*}{\partial z^*}\right)^2\right)}{T^*}. \tag{6c}$$

One notes that in the above equations T^* is measured in Kelvin. It is worth noting that the Bejan number, *Be*, is defined as the ratio of HTI to the total entropy generation rate as

$$Be = \frac{\mathrm{HTI}}{\mathrm{FFI} + \mathrm{HTI}}. \tag{6d}$$

For the case of negligible FFI, i.e. FFI =0, the Bejan number tends to become unity and one verifies that the only means of entropy generation is HTI. According to Bejan [15], for some special cases, one must include FFI in entropy generation analysis even if one has already neglected the viscous dissipation term in the thermal energy equation which is exactly the present case.

3. Solution procedure

3.1. Case 1

For this case we recover the analytical solution reported in [11] that proposes the following form for the longitudinal temperature gradient:

$$\frac{\partial T^*}{\partial x^*} = \frac{q''}{\rho c_P H U}\left(\frac{a+1}{a}\right). \tag{7}$$

The dimensionless temperature profile, $\theta = k\frac{T_w - T^*}{q'' D_H}$, may be rearranged as

$$\theta = \left(\frac{a+1}{2as}\right)^2 \frac{1}{A} \sum_{n=1}^{\infty} \frac{D_n}{\lambda_n^2} \cos \lambda_n y \left(s^2 - m^2 \frac{\cosh \lambda_n z}{\cosh \lambda_n a} + \lambda_n^2 \frac{\cosh mz}{\cosh ma}\right). \tag{8}$$

The dimensionless form of entropy generation, *Ns*, is defined to be

$$Ns = \frac{\dot{S}_{gen}}{k}\left(\frac{H}{q^*}\right)^2, \tag{9}$$

where the dimensionless heat flux, q^*, is

$$q^* = \frac{q'' D_H}{k T_w}. \tag{10}$$

We fixed the q^* value to $q^* = 0.1$ in this work so that one can neglect possible changes in the fluid and solid matrix physical property as a result of high temperature differences in a cross-section. In particular from Eqs. (6)–(10) one finds *Ns* and *Be* as

$$Ns = \frac{\left(\frac{a+1}{a}\right)^2 + \left(\frac{\partial \theta}{\partial y}\right)^2 + \left(\frac{\partial \theta}{\partial z}\right)^2}{(1 - \theta q^*)^2} + Br^* s^2 \frac{\phi}{(1 - \theta q^*)}, \tag{11a}$$

$$Be = \frac{\left(\frac{a+1}{a}\right)^2 + \left(\frac{\partial \theta}{\partial y}\right)^2 + \left(\frac{\partial \theta}{\partial z}\right)^2}{\left(\frac{a+1}{a}\right)^2 + \left(\frac{\partial \theta}{\partial y}\right)^2 + \left(\frac{\partial \theta}{\partial z}\right)^2 + Br^* s^2 (1 - \theta q^*)\phi}, \tag{11b}$$

where the modified Brinkman number, Br^*, is defined as

$$Br^* = \frac{\mu U^2}{k T_w q^{*2}}. \tag{11c}$$

Moreover, the dimensionless viscous dissipation function, ϕ, is defined as

$$\phi = \hat{u}^2 + s^{-2}\left(\left(\frac{\partial \hat{u}}{\partial y}\right)^2 + \left(\frac{\partial \hat{u}}{\partial z}\right)^2\right). \tag{12}$$

It is worth noting that ϕ remains unchanged while FFI changes from one case to another. All of the terms in Eqs. (11) and (12) are known and one may find both *Be* and *Ns* by Eqs. (11a) and (11b). The average values may be found as $Ns^* = \langle Ns \rangle$ and $Be^* = \langle Be \rangle$. Numerical integration is applied to find Ns^* and Be^* values since one notes that both *Ns* and *Be* are nonlinear functions of *y* and *z* and analytical solutions to the above equations are not possible.

3.2. Case 2

All three walls are kept at a uniform temperature (T_w) while the fourth one (the right wall shown in Fig. 1) is adiabatic. For this case the first law implies that

$$\frac{\partial T^*}{\partial x^*} = \frac{q''}{\rho c_P H U}\left(\frac{2a+1}{2a}\right). \tag{13}$$

Applying the dimensionless temperature profile, the thermal energy equation becomes

$$\frac{\partial^2\theta}{\partial y^2} + \frac{\partial^2\theta}{\partial z^2} + \frac{\hat{u}(a+1)(2a+1)}{8a^2} = 0. \tag{14}$$

The thermal boundary conditions are $\frac{\partial\theta}{\partial z} = 0$ at the adiabatic wall and $\theta = 0$ at other walls. The solution to Eq. (14) subject to the aforementioned boundary conditions may be written as

$$\theta = \sum_{n=1} f_n(z)\cos\lambda_n y. \tag{15}$$

After some algebraic manipulation one finds that

$$\theta = \frac{(a+1)(2a+1)}{16s^2a^2}\frac{\pi}{A}\sum_{n=1}^{\infty}\frac{(-1)^{n-1}}{\lambda_n^2}\left(A_1\cosh\lambda_n z + A_2\sinh\lambda_n z + \frac{\left(s^2+\lambda_n^2\frac{\cosh mz}{\cosh ma}\right)}{\lambda_n m^2}\right)\cos\lambda_n y \tag{16a}$$

with

$$A_1 = \frac{\lambda_n^2\tanh 2\lambda_n a\left(\frac{\tanh\lambda_n a}{2\lambda_n} - \frac{\tanh ma}{2m}\right) - 1}{\lambda_n^2\cosh\lambda_n a}, \tag{16b}$$

$$A_2 = \frac{\cosh\lambda_n a\left(\frac{\tanh\lambda_n a}{\lambda_n} - \frac{\tanh ma}{m}\right)}{\cosh 2\lambda_n a}. \tag{16c}$$

The compatibility condition (an identity resulting from the definitions)

$$Nu = \frac{1}{\langle\hat{u}\theta\rangle}, \tag{17}$$

yields an expression for the Nusselt number, namely

$$Nu = \frac{(2a\pi As)^2}{(2a+1)(a+1)}\Bigg/\sum_{n=1}^{\infty}\frac{K_n}{(2n-1)^4m^4}, \tag{18}$$

where

$$K_n = \frac{\lambda_n^2}{2}\tanh^2 ma - \left(\frac{\lambda_n^2}{2}-s^2\right)\left(1-\frac{\tanh ma}{ma}\right) + \frac{m^4}{2s^2}\left(\frac{\tanh\lambda_n a}{\lambda_n} - \frac{\tanh ma}{m}\right)\left(\lambda_n\tanh 2\lambda_n a\left(\frac{\tanh\lambda_n a}{\lambda_n} - \frac{\tanh ma}{m}\right) - 2\right). \tag{19}$$

The second law proposes the following form for *Ns* and *Be*:

$$Ns = \frac{\left(\frac{2a+1}{2a}\right)^2 + \left(\frac{\partial\theta}{\partial y}\right)^2 + \left(\frac{\partial\theta}{\partial z}\right)^2}{(1-\theta q^*)^2} + Br^* s^2\frac{\phi}{(1-\theta q^*)}, \tag{20a}$$

$$Be = \frac{\left(\frac{2a+1}{2a}\right)^2 + \left(\frac{\partial\theta}{\partial y}\right)^2 + \left(\frac{\partial\theta}{\partial z}\right)^2}{\left(\frac{2a+1}{2a}\right)^2 + \left(\frac{\partial\theta}{\partial y}\right)^2 + \left(\frac{\partial\theta}{\partial z}\right)^2 + Br^* s^2(1-\theta q^*)\phi}. \tag{20b}$$

3.3. Case 3

For this case it is assumed that the upper and lower walls are kept at a uniform temperature (T_w) while the sidewalls are adiabatic. The first law of thermodynamics implies

$$\frac{\partial T^*}{\partial x^*} = \frac{q''}{\rho c_P H U}. \tag{21}$$

In dimensionless form, the thermal energy equation reads

$$\frac{\partial^2\theta}{\partial y^2} + \frac{\partial^2\theta}{\partial z^2} + \frac{\hat{u}(a+1)}{4a} = 0. \tag{22}$$

The appropriate boundary conditions are $\theta = 0$ at the upper and lower walls and $\frac{\partial\theta}{\partial z} = 0$ at the adiabatic walls (sidewalls). One finds the dimensionless temperature distribution as

$$\theta = \frac{a+1}{4aA}\sum_{n=1}^{\infty}\frac{D_n}{\lambda_n^2}\left(1 - \frac{\lambda_n m\tanh ma}{s^2}\frac{\cosh\lambda_n z}{\sinh\lambda_n a} + \frac{\lambda_n^2}{s^2}\frac{\cosh mz}{\cosh ma}\right)\cos\lambda_n y, \tag{23}$$

and consequently one finds the Nusselt number as

$$Nu = \frac{2(\pi As)^2 a}{(a+1)}\Bigg/\sum_{n=1}^{\infty}\frac{F_n}{(2n-1)^4m^4}, \tag{24}$$

where

$$F_n = \left(\frac{\lambda_n^2}{2}-s^2\right)\left(1-\frac{\tanh ma}{ma}\right) - \frac{m^4}{s^2}\frac{\tanh ma}{m}\times\left(1-\frac{\lambda_n}{m}\frac{\tanh ma}{\tanh\lambda_n a}\right) + \frac{\lambda_n^2}{2}\tanh^2 ma. \tag{25}$$

Similar to the previous section, *Ns* and *Be* are found to be

$$Ns = \frac{1 + \left(\frac{\partial\theta}{\partial y}\right)^2 + \left(\frac{\partial\theta}{\partial z}\right)^2}{(1-\theta q^*)^2} + Br^* s^2\frac{\phi}{(1-\theta q^*)}, \tag{26a}$$

$$Be = \frac{1 + \left(\frac{\partial\theta}{\partial y}\right)^2 + \left(\frac{\partial\theta}{\partial z}\right)^2}{1 + \left(\frac{\partial\theta}{\partial y}\right)^2 + \left(\frac{\partial\theta}{\partial z}\right)^2 + Br^* s^2(1-\theta q^*)\phi}. \tag{26b}$$

4. Results and discussion

Closed form solutions have been obtained for the variation of velocity, temperature, the Bejan number, and the dimensionless entropy generation function throughout the solution domain. In the interest of brevity, we will limit our results to the effect of the duct aspect ratio and shape parameter on *Nu*, *Be*, and *Ns*.

Fig. 2 shows the Nusselt number for all the three cases studied versus the shape parameter. As a common trend, *Nu* seems to increase with the aspect ratio, *a*. One should, however, note that this trend is primarily due to the choice of the length scale in the definition of *Nu*. If the Nusselt number were based on $4H$, for example, instead of the

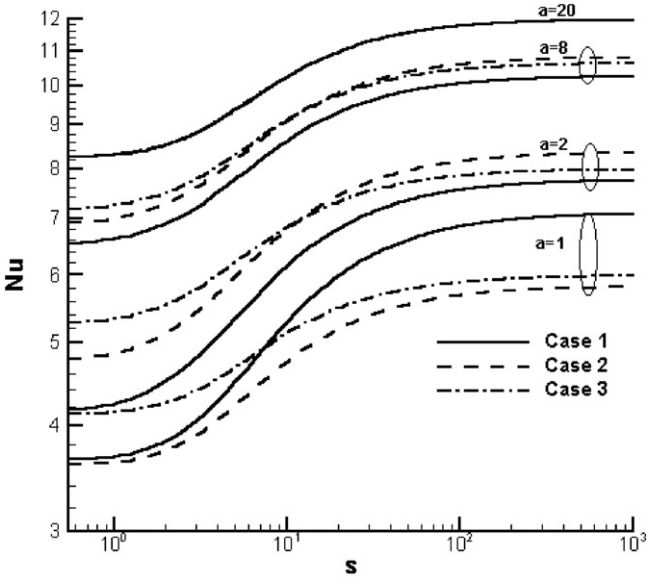

Fig. 2. The Nusselt number versus the porous media shape parameter for the three cases with some aspect ratios.

hydraulic diameter, D_H, the dependence on the aspect ratio would almost completely disappear. This shows the importance of recognizing the way the dimensionless parameters are constructed when interpreting the physical implications of graphs such as Fig. 2. The values at the low end of the s axis are expected to converge to the clear fluid conditions as porous medium permeability increases. In fact, they do so below $s = 1$ and show evidence of very good agreement against values reported in the literature for heat transfer in rectangular ducts with clear fluids, e.g. [28]. It is interesting to note that Shah and London [28] also based the Nusselt number on the hydraulic diameter, which emphasizes the dependence on the aspect ratio as mentioned above. The values at the high end of the s axis should approach the Darcy flow conditions. In fact, the Nusselt number seems to attain its Darcy flow value at around $s = 50$–70 regardless of neither the aspect ratio nor the boundary conditions. For s values approximately between 1 and 70, Nu has a power relation with s, increasing from its clear fluid value to almost its slug flow limit over this range. When examining the differences due to the heat transfer boundary conditions, one should remember that the heat flux in the Nusselt number definition (Eqs. (5a) and (5b)) is based on the heated perimeter rather than the wetted perimeter. This follows the general practice to facilitate comparison against past results reported in the literature [28–30]. It appears that the case 1 boundary condition almost always results in the lowest Nusselt number at the clear fluid end (as s approaches 0) of all three boundary condition cases. The only exception is for the square duct ($a = 1$), where Nu_2 values are consistently below the other two cases over entire s domain, but even there the clear fluid values for cases 1 and 2 are very close to each other. In general, for small s values Nu_3 is higher than Nu_1 while for higher s values it is the other way around. For clear fluid or hyperporous flow through square ducts, case 3 results in a higher Nu value with the same pressure drop. As s increases for a square duct, e.g. keeping a fixed duct size when the permeability is lowered, case 1 provides the highest Nusselt number. In addition to having a higher Nusselt number over the heat transfer area, it should be remembered that the actual heat transfer area is also higher for the case 1 boundary condition. Therefore, flow through a square duct with low permeability achieves the best heat removal rates under case 1 boundary conditions. This fact may be of vital importance when it comes to applications such as low permeability foam for cooling electronic equipment similar to the Al-foam examined by Lage et al. [31]. However, with rectangular cross-sections, the situation starts changing in such a way that Nu_1 goes to minimum regardless of the s value. Considering rectangular porous passages with small s values, Nu_3 is always higher than the other two. On the other hand, for higher s values approaching slug flow conditions, Nu_2 exceeds Nu_3 (and Nu_1 non-square ducts). This does not change the fact that if one needs to achieve maximum cooling rate, all four surfaces must be used. However, our results show that there is some compensation offered by higher Nu values over smaller heat transfer areas if one has to limit the heat exchange area for other reasons.

Another point worth mentioning is that for very large aspect ratios, all of the three cases resemble parallel plate channel case where the Nu plots become almost indistinguishable. This is expected since for very large values of a, heat transfer rate from the two short sidewalls is negligible compared to the total heat transfer rate.

To explain the Nu behavior, we classify the results in terms of high ($s \gg 10$) and low porous media shape parameters ($s \ll 10$). For small s values, case 3 achieves the highest Nu values. This case has two adiabatic walls near which the temperature shows no change in the direction normal to the walls. This means that in this region the heat transfer is almost one dimensional (along the side walls) and the temperature is not equal to T_w. This means that the minimum temperature, which is expected to happen in the duct center for being in its farthest distance from the walls, is higher than the minimum value for the other two cases when the heat input to the duct as our thermodynamic system (which will change the enthalpy of the system) is constant for the three cases. Considering the fact that in the duct center the velocity experiences its maximum, one expects that the bulk-wall temperature difference (which is inversely proportional to Nu) be minimum compared to the other counterparts leading to an increase in Nu. However, when s increases to higher values, say $s > 10$, the velocity changes are restricted to thin near wall regions [11] and out of this region the velocity distribution is uniform. For large s values there are two opposing effects: near the adiabatic walls the heat transfer is one dimensional and this enhances the minimum temperature at the duct center compared to a case with no adiabatic wall, i.e. case 1. On the other hand, high near wall temperatures when one

has heated walls are associated with small velocity values due to wall effects. Case 2 lies somewhere between the two others in such a way that near the adiabatic wall isotherms of case 2 become similar to that of case 3 which happens only near the heated wall which resembles case 1. It seems that for this reason case 2 leads to higher *Nu* values for rectangular cross-sections when the porous media shape parameter is large. When it comes to a square cross-section, case 1 delivers the highest Nusselt number and this is justified when one observes that the diagonal lines are adiabatic lines along which no heat is transferred and isotherms are normal to these lines, similar to a pure conduction problem. This will lead to circular temperature distribution which is more uniform compared to the other cases since, to a good extent, the duct cross-section can be considered as sum of 8 similar triangles each of which formed by two adiabatic lines and half of a wall. In a nutshell, the center-wall temperature difference is smaller than the other cases with a net effect of decreasing wall-bulk temperature difference and increasing *Nu*. However, with rectangular cross-sections, the diagonal symmetry will no more exist for case 1.

Fig. 3a and b show Ns^* versus a for $s = 1$ and $s = 10$, respectively. A quick check of both figures shows that the dimensionless average entropy generation rate appears to be decreasing with an increase in the duct aspect ratio regardless of the s value. As it was already noted for the Nusselt number above, the choice of the length scale must be recognized in interpreting these results. To facilitate comparisons with past literature, the non-dimensional entropy generation is based on the hydraulic diameter as shown in Eqs. (9) and (10). The dimensionless entropy generation is higher for the square cross-section compared to the rectangular counterparts and this is similar to what reported by previous researchers [17,32]. Moreover, comparing the Ns^* levels in the two figures, one realizes that increasing s increases Ns^*. Another feature of considerable interest is that, regardless of s and a value, case 1 is the most irreversible design while case 3 produces the least entropy. In the view of the above, one concludes that the least efficient design is case 1 with $a = 1$ and $s = 10$. For this reason we gave this case a special attention within the rest of our study.

Fig. 4a and b shows the line diagrams of *Be* and *Ns* for a better understanding of the problem. Fig. 4a illustrates *Be* versus y at four z locations. One observes that *Be* is more or less constant excluding a thin near wall region where for $z = 0.9$, *Be* reaches its maximum value while at smaller z, *Be* increases and then decreases to its minimum value at the wall. It is also clear that in this case, *Be* is less than 0.5 and hence FFI > HTI. This is an expected result since in this case s is large enough to allow FFI to become comparable to HTI.

Comparing Fig. 4b with the previous one, one observes that *Ns* plots are in opposite direction to those of *Be* in such a way that the maximums/minimums of *Ns* are associated with the minimums/maximums of *Be*. With $z = 0.9$,

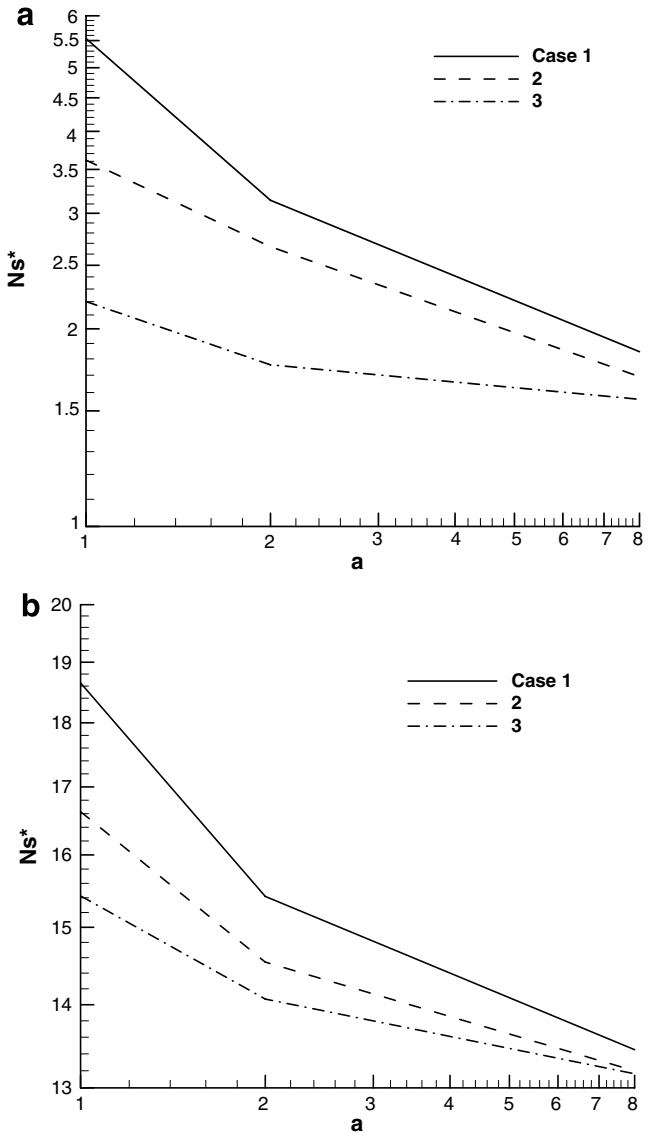

Fig. 3. Average dimensionless entropy generation for the three cases versus the aspect ratio, (a) $s = 1$ and (b) $s = 10$.

the value of *Ns* increases from wall to the duct center while at other z locations *Ns* decreases from the wall to a near-wall minimum, increasing and then remaining constant up to the duct center. According to this figure, the walls are the most active entropy generation sites where both of the temperature and velocity gradients experience their maximum values and consequently both HTI and FFI increase with the net effect of increasing *Ns*. One notes that *Ns* value at the duct center is not a minimum one. This fact is unique for a porous passage and in the clear fluid case one expects *Ns* to be at minimum since both velocity and temperature gradients vanish due to symmetry. A quick check of the *Ns* function shows that moving from the walls to the channel center, the Darcy dissipation term (which is absent in the clear fluid case) will grow due to the diminishing boundary effects and hence FFI, which is proportional to u^2. More on the topic can be found in recent notes on

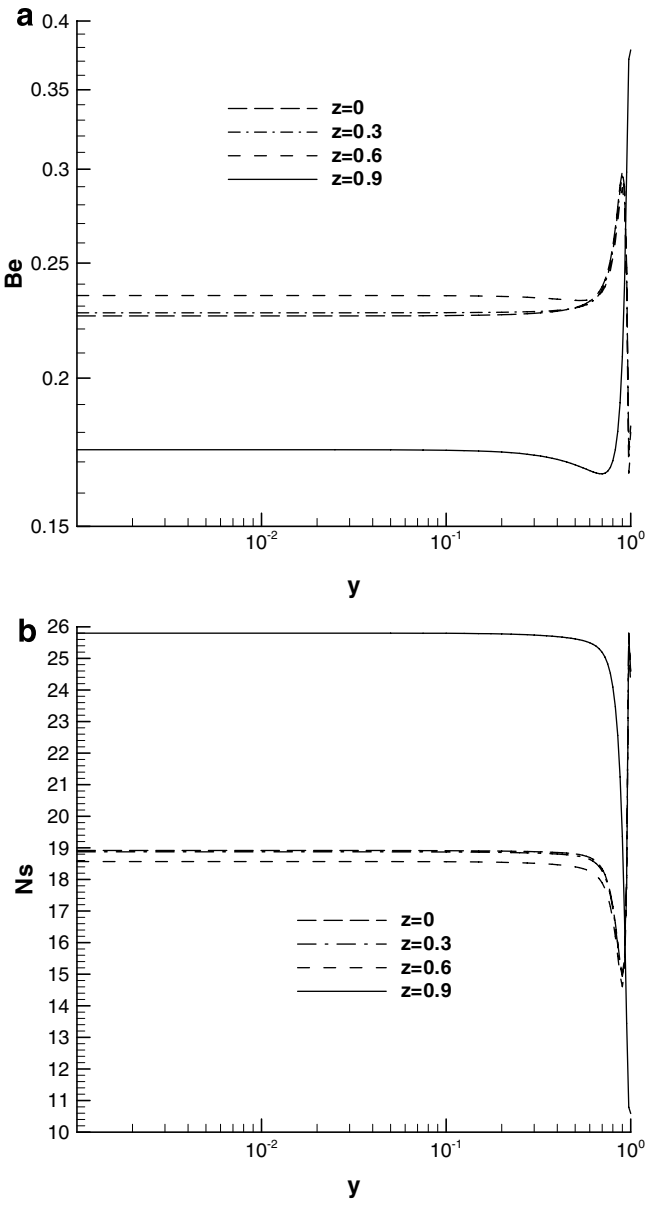

Fig. 4. (a) Local Bejan number and (b) local dimensionless entropy generation for case 1 with $s = 10$ for a duct of square cross-section.

viscous dissipation in a duct clear of solid materials [33] and viscous dissipation in ducts filled by a porous medium [34].

One of the reviewers has raised the question for the basis of the neglect of the viscous dissipation effects in the thermal energy equation while the FFI term in the entropy generation function is retained. We follow the same approach as Bejan [15, p. 102] to answer this question. Order of magnitude analysis in the thermal energy equation leads to the fact that the Brinkman number $\left(Br = \frac{\mu U^2 H}{q'' K}\right)$ is the key parameter to decide on the importance of viscous dissipation, see Nield [34–36]. On the other hand, observing Eqs. (11a), (20a), and (26a), one realizes that $Br^* s^2$ shows the relative importance of FFI/HTI or the role played by viscous dissipation, through FFI, in the second law. The relative importance of these two key parameters can be reflected in a parameter, say B^*, as

$$B^* = \mathrm{O}\left(\frac{\left(\frac{\mu U^2 H}{q'' K}\right)_{\text{1stlaw}}}{\left(\frac{\mu U^2}{k T_w q^{*2}} s^2\right)_{\text{2ndlaw}}}\right). \tag{27}$$

This can be rearranged as

$$B^* = \mathrm{O}\left(\frac{k T_w q^{*2}}{q'' H}\right). \tag{28}$$

Using Eq. (10) and replacing for D_H, one has

$$B^* = \mathrm{O}\left(\frac{4a}{a+1} q^*\right). \tag{29}$$

Or simply $B^* = \mathrm{O}(q^*)$ and as we assumed $q^* = 0.1$, $B^* = \mathrm{O}(0.1)$. This gives us the impression that the relative importance of viscous dissipation in the first law to that of the second law is O(0.1). This is also in line with Bejan's [15] final conclusion, as expected.

5. Conclusion

The objective of the present study is to optimize heat transfer in rectangular porous ducts via both first and second laws of thermodynamics. Analytical solutions are reported for the temperature distribution and the Nusselt number that envelop three different boundary conditions. Our closed form solutions can be used for benchmark checks on numerical findings for flow in parallel plate channels or ducts of rectangular cross-section filled with or without a porous matrix. This is a relatively important topic as reflected by the amount of numerical work addressing similar issues; see for example [37–42]. It is found that for $s < 10$ the best use of the heat transfer area in view of the best heat transfer rate (with the same pressure drop) is achieved by case 3. However, for $s > 10$ the optimum design is dependent on a value in such a way that for a duct of square cross-section, case 1 acts better than the others while for other values of a, case 2 provides the best heat transfer rate. Having known the velocity and temperature profile, the second law analysis of the problem is presented. It is found that case 3 is the best design for having the minimal lost work, with the same a and s values, while case 1 is associated with the highest entropy production value among the others.

Acknowledgments

The first author, the scholarship holder, acknowledges the support provided by The University of Queensland in terms of UQILAS, Endeavor IPRS, and School Scholarship.

References

[1] A. Narasimhan, J.L. Lage, Modified Hazen–Dupuit–Darcy model for forced convection of a fluid with temperature-dependent viscosity, ASME J. Heat Transfer 123 (2001) 31–38.

[2] D.A. Nield, A. Bejan, Convection in Porous Media, third ed., Springer, New York, 2006.

[3] P. Cheng, Heat transfer in geothermal systems, Adv. Heat Transfer 14 (1978) 1–105.

[4] A. Haji-Sheikh, K. Vafai, Analysis of flow and heat transfer in porous media imbedded inside various-shaped ducts, Int. J. Heat Mass Transfer 47 (2004) 1889–1905.

[5] A. Haji-Sheikh, Fully developed heat transfer to fluid flow in rectangular passages with filled with porous materials, ASME J. Heat Transfer 128 (2006) 822–828.

[6] A. Haji-Sheikh, W.J. Minkowycz, E.M. Sparrow, Green's function solution of temperature field for flow in porous passages, Int. J. Heat Mass Transfer 47 (2004) 4685–4695.

[7] A. Haji-Sheikh, D.A. Nield, K. Hooman, Heat transfer in thermal entrance region for flow through rectangular porous passages, Int. J. Heat Mass Transfer 49 (2006) 3004–3015.

[8] A. Haji-Sheikh, W.J. Minkowycz, E.M. Sparrow, A numerical study of the heat transfer to fluid flow through circular porous passages, Numer. Heat Transfer A 46 (2004) 929–955.

[9] A. Haji-Sheikh, E.M. Sparrow, W.J. Minkowycz, Heat transfer to flow through porous passages using extended weighted residuals method – a Green's function solution, Int. J. Heat Mass Transfer 48 (2005) 1330–1349.

[10] A. Haji-Sheikh, Estimation of average and local heat transfer in parallel plates and circular ducts filled with porous materials, ASME J. Heat Transfer 126 (2004) 400–409.

[11] K. Hooman, A.A. Merrikh, Analytical solution of forced convection in a duct of rectangular cross-section saturated by a porous medium, ASME J. Heat Transfer 128 (2006) 596–600.

[12] K. Hooman, Fully developed temperature distribution in a porous saturated duct of elliptical cross-section, with viscous dissipation effects and entropy generation analysis, Heat Transfer Res. 36 (2005) 237–245.

[13] K. Hooman, Analysis of entropy generation in porous media imbedded inside elliptical passages, Int. J. Heat Technol. 23 (2005) 145–149.

[14] K. Hooman, H. Gurgenci, Effects of temperature-dependent viscosity variation on entropy generation, heat, and fluid flow through a porous-saturated duct of rectangular cross-section, Appl. Math. Mech. – English Edition 28 (1) (2007), in press.

[15] A. Bejan, Entropy Generation through Heat and Fluid Flow, Wiley, New York, 1982.

[16] I. Dagtekin, H.F. Oztop, A.Z. Sahin, An analysis of entropy generation through a circular duct with different shaped longitudinal fins for laminar flow, Int. J. Heat Mass Transfer 48 (2005) 171–181.

[17] E.B. Ratts, A.G. Raut, Entropy generation minimization of fully developed internal flow with constant heat flux, ASME J. Heat Transfer 126 (2004) 656–659.

[18] A.C. Baytas, Entropy generation for natural convection in an inclined porous cavity, Int. J. Heat Mass Transfer 43 (2000) 2089–2099.

[19] A.C. Baytas, Entropy generation for free and forced convection in a porous cavity and a porous channel, in: D.B. Ingham et al. (Eds.), Emerging Technology and Techniques in Porous Media, Kluwer Academic Publishers, Dordrecht, 2004, pp. 259–270.

[20] D.A. Nield, Resolution of a paradox involving viscous dissipation and nonlinear drag in a porous medium, Transport Porous Med. 41 (2000) 349–357.

[21] A.K. Al-Hadrami, L. Elliott, D.B. Ingham, A new model for viscous dissipation in porous media across a range of permeability values, Transport Porous Med. 53 (2003) 17–122.

[22] D.A. Nield, A.V. Kuznetsov, M. Xiong, Effects of viscous dissipation and flow work on forced convection in a channel filled by a saturated porous medium, Transport Porous Med. 56 (2004) 351–367.

[23] K. Hooman, H. Gurgenci, Effects of viscous dissipation and boundary conditions on forced convection in a channel occupied by a saturated porous medium, Transport Porous Med., in press, doi:10.1007/S11242-006-9049-4.

[24] K. Hooman, A. Pourshaghaghy, A. Ejlali, Effects of viscous dissipation on thermally developing forced convection in a porous saturated circular tube with an isoflux wall, Appl. Math. Mech. (English edition) 27 (2006) 617–626.

[25] D.A. Nield, Comments on 'A new model for viscous dissipation in porous media across a range of permeability values' by A.K. Al-Hadrhrami, L. Elliott and D.B. Ingham, Transport Porous Med. 55 (2004) 253–254.

[26] K. Hooman, A. Ejlali, Second law analysis of laminar flow in a channel filled with saturated porous media: a numerical solution, Entropy 7 (2005) 300–307.

[27] K. Hooman, A.A. Merrikh, A. Ejlali, Comments on "Flow, thermal, and entropy generation characteristics inside a porous channel with viscous dissipation" by S. Mahmud and R.A. Fraser, Int. J. Thermal Sci., in press.

[28] R.K. Shah, A.L. London, Laminar Flow Forced Convection in Ducts (Advances in Heat Transfer, Supplement 1), Academic Press, New York, 1978.

[29] A. Bejan, I. Dincer, S. Lorente, A.F. Miguel, A.H. Reis, Porous and Complex Flow Structures in Modern Technology, Springer, New York, 2004.

[30] A. Bejan, Advanced Engineering Thermodynamics, second ed., Wiley, New York, 1997.

[31] J.L. Lage, B.V. Antohe, D.A. Nield, Two types of nonlinear pressure-drop versus flow rate observed for saturated porous media, ASME J. Fluids Eng. 119 (1997) 700–706.

[32] A.Z. Sahin, Irreversibilities in various duct geometries with constant wall heat flux and laminar flow, Energy 23 (1998) 465–473.

[33] D.A. Nield, K. Hooman, Comments on "Effects of viscous dissipation on the heat transfer in forced pipe flow. Part 1: both hydrodynamically and thermally fully developed flow and Part 2: thermally developing flow" by O. Aydin, Energy Convers. Manage. 47 (2006) 3501–3503.

[34] D.A. Nield, A note on a Brinkman–Brinkman forced convection problem, Transport Porous Med. 64 (2006) 185–188.

[35] D.A. Nield, Modelling fluid flow in saturated porous media and at interfaces, in: D.B. Ingham, I. Pop (Eds.), Transport Phenomena in Porous Media II, Elsevier, Oxford, 2002, pp. 1–19.

[36] D.A. Nield, The modeling of viscous dissipation in a saturated porous medium, ASME J. Heat Transfer (submitted for publication).

[37] S.S. Mousavi, K. Hooman, Heat and fluid flow in entrance region of a channel with staggered baffles, Energy Convers. Manage. 47 (2006) 2011–2019.

[38] P.C. Huang, K. Vafai, Internal heat transfer augmentation in a channel using an alternate set of porous cavity block obstacles, Numer. Heat Transfer A 25 (1994) 519–539.

[39] A.V. Kuznetsov, L. Cheng, M. Xiong, Effects of thermal dispersion and turbulence in forced convection in a composite parallel-plate channel: investigation of constant wall heat flux and constant wall temperature cases, Numer. Heat Transfer A 42 (2002) 365–383.

[40] J. Facao, A.C. Oliveira, Modeling laminar heat transfer in a curved rectangular duct with a computational fluid dynamics code, Numer. Heat Transfer A 48 (2005) 165–177.

[41] A. Narasimhan, J.L. Lage, Forced convection of a fluid with temperature-dependent viscosity flowing through a porous medium channel, Numer. Heat Transfer A 40 (2001) 801–820.

[42] A.V. Kuznetsov, D.A. Nield, Effects of heterogeneity in forced convection in a porous medium: Triple layer or conjugate problem, Numer. Heat Transfer A 40 (2001) 363–385.